OXFORD

Human Molecular Genetics, 2022, Vol. 31, 15, 2639–2654
https://doi.org/10.1093/hmg/ddac010
Advance access publication date: 25 March 2022
Original Article

XBP1 variant 1 promotes mitosis of cancer cells involving upregulation of the polyglutamylase TTLL6

Yongwang Zhong[1,2], Wenjing Yan[1,2], Jingjing Ruan[1,3], Mike Fang[4], Changjun Yu[5], Shaojun Du[6], Ganesha Rai[7], Dingyin Tao[7], Mark J. Henderson[7] and Shengyun Fang[1,2,6,8,*]

[1]Center for Biomedical Engineering and Technology, University of Maryland School of Medicine, Baltimore, MD 21201, USA
[2]Department of Physiology, University of Maryland School of Medicine, Baltimore, MD 21201, USA
[3]Department of Pulmonary Medicine, Anhui Medical University First Affiliated Hospital, Hefei, Anhui 230032, China
[4]Population and Quantitative Health Sciences Department, Case Western Reserve University, Cleveland, OH 44106, USA
[5]Department of General surgery, Anhui Medical University First Affiliated Hospital, Hefei, Anhui 230032, China
[6]Department of Biochemistry and Molecular Biology, University of Maryland School of Medicine, Baltimore, MD 21201, USA
[7]National Center for Advancing Translational Sciences, National Institutes of Health, Rockville, MD 20850, USA
[8]Program in Oncology, UM Greenebaum Comprehensive Cancer Center, University of Maryland School of Medicine, Baltimore, MD 21201, USA
*To whom correspondence should be addressed at: Center for Biomedical Engineering and Technology, University of Maryland School of Medicine, 111 S. Penn St, Room 307A, Baltimore, MD 21201, USA. Tel: 401-706-2220; Fax: 410-706-8184; Email: sfang@som.umaryland.edu

Abstract

XBP1 variant 1 (Xv1) is the most abundant XBP1 variant and is highly enriched across cancer types but nearly none in normal tissues. Its expression is associated with poor patients' survival and is specifically required for survival of malignant cells, but the underlying mechanism is not known. Here we report that Xv1 upregulates the polyglutamylase tubulin tyrosine ligase-like 6 (TTLL6) and promotes mitosis of cancer cells. Like the canonical XBP1, Xv1 mRNA undergoes unconventional splicing by IRE1α under endoplasmic reticulum stress, but it is also constitutively spliced by IRE1β. The spliced Xv1 mRNA encodes the active form of Xv1 protein (Xv1s). RNA sequencing in HeLa cells revealed that Xv1s overexpression regulates expression of genes that are not involved in the canonical unfolded protein response, including TTLL6 as a highly upregulated gene. Gel shift assay and chromatin immunoprecipitation revealed that Xv1s bind to the TTLL6 promoter region. Knockdown of TTLL6 caused death of cancer cells but not benign and normal cells, similar to the effects of knocking down Xv1. Moreover, overexpression of TTLL6 partially rescued BT474 cells from apoptosis induced by either TTLL6 or Xv1 knockdown, supporting TTLL6 as an essential downstream effector of Xv1 in regulating cancer cell survival. TTLL6 is localized in the mitotic spindle of cancer cells. Xv1 or TTLL6 knockdown resulted in decreased spindle polyglutamylation and interpolar spindle, as well as congression failure, mitotic arrest and cell death. These findings suggest that Xv1 is essential for cancer cell mitosis, which is mediated, at least in part, by increasing TTLL6 expression.

Introduction

Microtubules (MTs) are formed by polymerization of α- and β-tubulins. Posttranslational modifications, such as detyrosination/retyrosination, (poly) glutamylation and (poly)glycylation constitute tubulin codes that regulate MT mechanical properties, dynamics and protein interactions (1,2). Of those modifications, polyglutamylation is the most evolutionarily conserved from ciliates to humans (1–3). It occurs via the addition of polyglutamyl side chains to glutamate residues within evolutionarily conserved C-terminal acidic motifs on both α- and β-tubulin (4). A family of seven tubulin tyrosine ligase-like (TTLL) enzymes catalyze this modification (2). Different TTLL enzymes have preference to modify either α- or β-tubulin and to either initiate or elongate glutamate chains (5). Both mono- and polyglutamylation can be reversed by a family of cytosolic carboxypeptidases(2).

Tubulin tyrosine ligase-like 6 (TTLL6) is a polyglutamylase that catalyzes extension of polyglutamyl side chains to regulate cellular activities, particularly cilia structure and motility (2,5–8). Overexpression of TTLL6 strongly increases polyglutamylation of MTs in the cilia axoneme and cell body of *Tetrahymena* and inhibits cell proliferation and ciliary dynein-based motility (7). Moreover, it stabilizes cytoplasmic MTs and destabilizes axonemal MTs, suggesting that spatially restricted interacting proteins may be responsible for these opposite activities (9). Deletion of the two TTLL6 paralogs in *Tetrahymena* causes severe deficiency in ciliary motility associated with abnormal waveform and reduced beat frequency (10). In zebrafish, TTLL6 knockdown decreases tubulin polyglutamylation and affects cilia structure and motility in olfactory placodes (11,12). The similar function of TTLL6 is likely conserved in mammalian cells (5). For example, TTLL6 is necessary for coordinated beating behavior of ependymal cilia in developing mouse brain (13). Mutation of regulators of TTLL6 entry into cilia causes ciliopathy-related phenotypes in human cells, zebrafish and mice and results in glutamylation defects in the ciliary axoneme (14,15). Mutation of CEP41, a

Received: August 9, 2021. **Revised:** December 19, 2021. **Accepted:** January 10, 2022

regulator of ciliary entry of TTLL6, causes Joubert syndrome characterized by cerebellar hypoplasia and neurological disorders (14). TTLL6 is also involved in amyloid-β-induced neuronal damage in models of Alzheimer's disease (6,16). Oligomerization of amyloid-β causes misssorting of tau into somatodendritic compartment of neurons, leading to TTLL6 mislocalization into the dendrites. TTLL6 then polyglutamylates MTs and triggers spastin-mediated severing of dendritic MTs, leading to decreases in MTs, a hallmark of Alzheimer's disease (6,16,17). TTLL6 also catalyzes polyglutamylation of non-tubulin substrate proteins. For example, TTLL6 catalyzes cyclic GMP-AMP synthase (cGAS) polyglutamylation, which inhibits its DNA binding and represses the innate immune response to viral infections (1,18). TTLL6 also catalyzes Mad2 polyglutamylation and plays a critical role in megakaryopoiesis (19).

XBP1 is a basic leucine zipper (bZIP) transcription factor and a key mediator of the endoplasmic reticulum (ER) stress-activated unfolded protein response (UPR). A unique mechanism of XBP1 regulation is the unconventional splicing of XBP1 mRNA to remove a 26-nucleotide intron by IRE1α RNase under ER stress (20,21). The splicing reaction creates a translational frameshift to enable encoding the functional transcription factor XBP1s. Recently, we reported a novel XBP1 variant, namely XBP1v1 (Xv1) (22). Xv1 is highly enriched in a large fraction of all cancer types found in the Cancer Genome Atlas (TCGA) database with little to no expression detected in normal tissues. Similarly, Xv1 is widely expressed in different cancer cell lines but not in normal and non-cancerous cells. Elevated Xv1 expression is associated with poor survival for patients with several types of cancer, including breast invasive carcinoma, pancreatic adenocarcinoma, liver hepatocellular carcinoma, sarcoma, bladder urothelial carcinoma and head and neck squamous cell carcinoma (22). Knockdown of Xv1 but not XBP1 causes death of various types of cancer cells but not normal and non-cancerous cells *in vitro*. Knockdown of Xv1 also inhibited breast cancer growth in mouse xenograft. These results suggest that Xv1 is specifically required for survival of cancer cells.

In this study, we found that Xv1 mRNA is constitutively spliced by IRE1β and also subject to ER stress-induced splicing by IRE1α. The spliced Xv1 mRNA (Xv1s) encodes the active Xv1s protein. Overexpression of Xv1s upregulates TTLL6 but does not regulate the canonical UPR. Further studies found that Xv1s regulates mitosis of cancer cells, at least in part, through TTLL6-mediated mitotic spindle polyglutamylation.

Results

Xv1 mRNA undergoes unconventional splicing by both IRE1α and IRE1β in cancer cells

Xv1 acquires a cryptic first exon to replace the exon 1 of XBP1 but shares all the downstream exons with the latter (22). Therefore, Xv1 mRNA has the same 26-nucleotide intron contained in XBP1 mRNA, and we predicted that the Xv1 transcript would undergo the same unconventional splicing as XBP1 mRNA (20,21). Using specific primers, both unspliced (Xv1u) and the spliced (Xv1s) forms of Xv1 mRNA were detected to various extents in all six cancer cell lines tested by reverse transcription polymerase chain reaction (RT-PCR) (Fig. 1A). Immunoblotting using a rabbit polyclonal antibody UMY162 that was raised against a common peptide in XBP1u/s and Xv1u/s proteins (see antigen peptide sequence in *Methods* section) confirmed that Xv1s protein is expressed as a doublet in all six cancer lines (Fig. 1B). The identity of Xv1s was validated by knockdown of Xv1 mRNA (Fig. 1C). These results suggest that Xv1 also undergoes unconventional splicing like XBP1.

Next, we determined the role of IRE1α in Xv1 splicing. HeLa cells that express low levels of Xv1s were treated with tunicamycin to induce ER stress, which activates IRE1α. The treatment resulted in a shift from Xv1u to Xv1s, as well as XBP1u to XBP1s, as shown in RT-PCR (Fig. 1D). Treatment with an IRE1α inhibitor, 4μ8C (23), abolished the effects of tunicamycin on both XBP1s and Xv1s (Fig. 1D). Immunoblotting also showed that, in BT474 cells that highly express Xv1s, tunicamycin treatment increased both XBP1s and Xv1s proteins, though to a much less extent for the latter (Fig. 1E). The increases in XBP1s and Xv1s proteins were reversed by 4μ8C treatment (Fig. 1E). These results indicate that Xv1 can be spliced by IRE1α under ER stress.

Unlike Xv1s that was readily detected under resting condition by immunoblotting in BT474 and other cancer cell lines tested, XBP1s was hardly detected in the same samples (Fig. 1B and E). It is known that both XBP1s and XBP1u are unstable proteins degraded by proteasome (24). Treatment of BT474 cells with proteasome inhibitor bortezomib (BTZ) but not autophagy inhibitor chloroquine increased the levels of XBP1u, Xv1u and Xv1s proteins, but had little effect on XBP1s protein (Fig. 1F). In addition, transient expression of Xv1 and XBP1 in HeLa cells resulted in much higher ratio of Xv1s/Xv1u than XBP1s/XBP1u (Fig. 1F, lanes 1 vs. 2, and G). These results indicate that Xv1 mRNA and, to a much less extent, the XBP1 mRNA are constitutively spliced in the cancer cells examined, resulting in translation of more Xv1s protein than XBP1s protein. Notably, 4μ8C treatment had little effect on basal Xv1s protein level in BT474 cells without tunicamycin treatment (Fig. 1F), suggesting that IRE1α is not responsible for Xv1 constitutive splicing.

IRE1α has a paralog, IRE1β, that has the same structural domains as IRE1α. In contrast to IRE1α, which is ubiquitously expressed, IRE1β expression is restricted to epithelial cells of the airway and digestive system (25,26). Mining gene expression datasets revealed that IRE1β but not IRE1α is upregulated in multiple cancer tissues as compared with normal control tissues (27) (Supplementary Material, Fig. S1). Previous

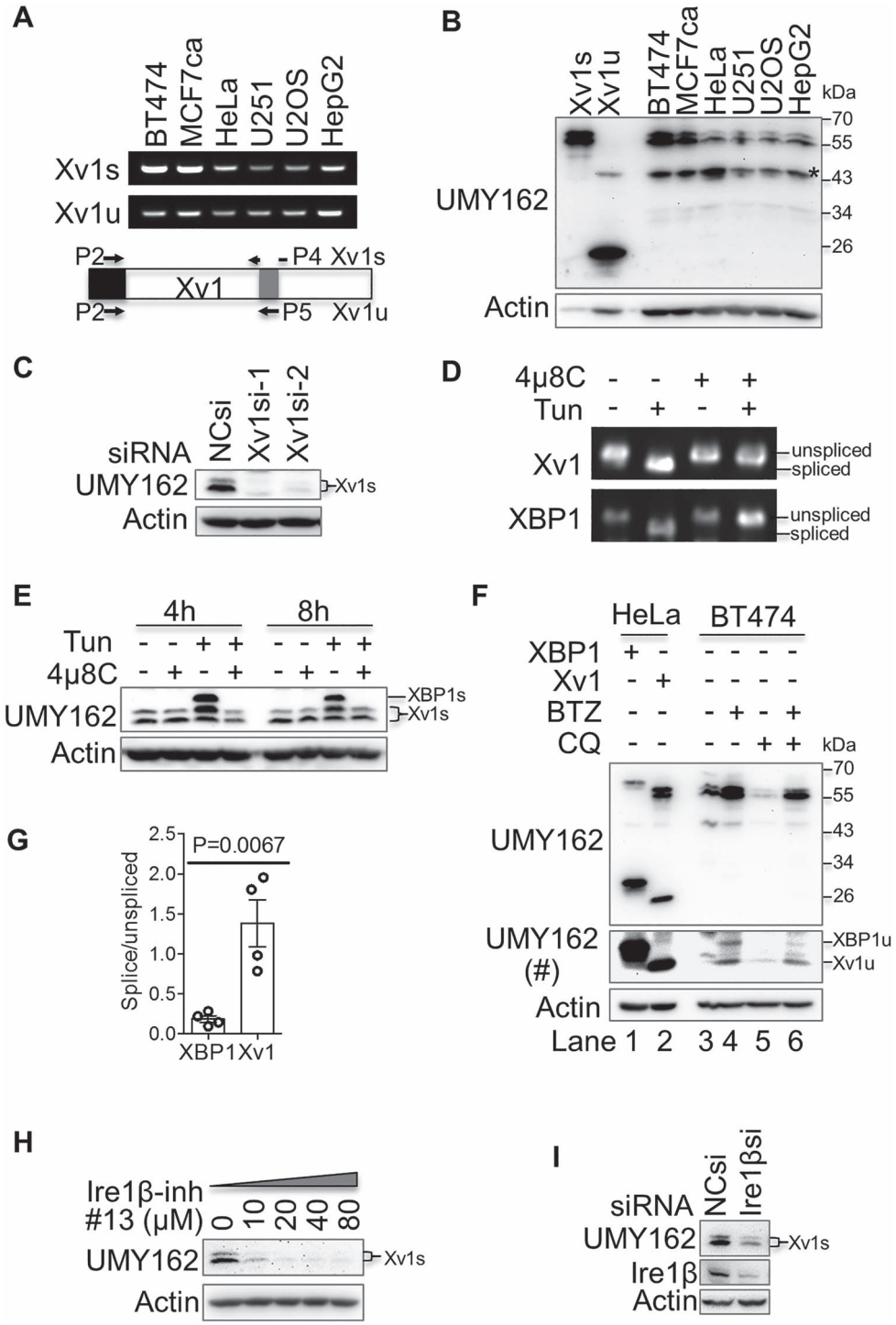

Figure 1. Xv1 is spliced by both Ire1α and Ire1β in cancer cells. (**A**) RT-PCR of spliced (Xv1s) and unspliced (Xv1u) Xv1 mRNA in cancer cell lines. Positions of specific primers used for Xv1s (P2 + P4) or Xv1u (P2 + P5) were shown in the diagram. (**B**) Immunoblotting of Xv1 in cancer cell lines. UMY162 antibody was generated against a common peptide in XBP1u/s and Xv1u/s proteins. Ectopically expressed Xv1s and Xv1u were used as controls. Asterisk indicates a non-specific band. (**C**) Immunoblotting of Xv1s in BT474 cells transfected with two different Xv1 siRNAs. (**D**) RT-PCR of HeLa cells treated with 4μ8C (25 μM) or tunicamycin (Tun, 2 μg/ml) for 2 h. XBP1 or Xv1 specific primers were used to detect unspliced and spliced forms simultaneously. Note that the spliced form runs faster than the unspliced form in the polyacrylamide gel electrophoresis for either XBP1 or Xv1. (**E**) Immunoblotting of BT474 cells treated with 4μ8C (25 μM) or tunicamycin (Tun, 2 μg/ml). (**F**) Immunoblotting of endogenous Xv1u and Xv1s in BT474 cells treated with BTZ (2 μM) or chloroquine (CQ, 50 μg/ml) as indicated for 4 h. HeLa cells transfected with XBP1 or Xv1 cDNA were used as controls. #, developed with higher sensitivity ECL substrate. (**G**) Ectopically expressed Xv1 is highly spliced. Xv1 or XBP1 was expressed in HeLa cells. The band densities of the spliced and unspliced forms were measured from the immunoblots. The ratios of the spliced form versus unspliced were plotted. $n = 4$. Unpaired t-test. (**H**) Inhibition of Ire1β decreases Xv1s protein. BT474 cells were treated with Ire1β inhibiter #13 (29) for overnight. (**I**) Knockdown of Ire1β decreases Xv1s protein in BT474 cells.

studies showed that IRE1α is activated by ER stress, whereas IRE1β is constitutively active (28). Thus, IRE1β may be responsible for the constitutive splicing of Xv1 in cancer cells (Fig. 1A and B). In support of this possibility, inhibition of IRE1β RNase by either a reported small molecule inhibitor (29) or knockdown of IRE1β expression decreased the basal levels of Xv1s protein in BT474 cells (Fig. 1H and I). Notably, no Xv1u proteins were detectable in IRE1β knockdown and IRE1β inhibitor treated cells (Fig. 1H and I), which is likely because of its degradation by the proteasome as seen in Fig. 1F. These data suggest that Xv1 mRNA is constitutively spliced by IRE1β in cancer cells.

Notably, the Xv1s band was detected migrating at two molecular weights (a doublet) in immunoblots (Fig. 1B and C) with the upper band more sensitive to tunicamycin treatment (Fig. 1E). Treatment of BT474 cell lysates with lambda protein phosphatase resulted in a shift to the lower molecular weight form, suggesting that the upper Xv1s protein band represents a phosphorylated species (Supplementary Material, Fig. S2A). To identify the phosphorylation site(s), Xv1s-HA was transiently expressed in HeLa cells and then immunoprecipitated. Mass spectrometry results showed that Xv1s-HA was phosphorylated at Thr73, Ser162, Ser238 and Ser240 (Supplementary Material, Fig. S2B). Mutagenesis analyses suggest that Ser162 is a principal phosphorylation site that is required for the observed mobility shift (Supplementary Material, Fig. S2C).

Xv1s is an active transcription factor that does not regulate the canonical UPR

To determine whether Xv1s is the active form of Xv1 that regulates cancer cell survival, we performed rescue experiments using siRNA-resistant complementary DNA (cDNA) encoding Xv1s or Xv1u in Xv1 knockdown BT474 cells. Transient transfection of Xv1s but not Xv1u cDNA efficiently rescued BT474 cell death in Xv1 depleted cells (Fig. 2A and B), suggesting that Xv1s promotes cancer cell survival.

Compared with XBP1s, Xv1s contains an identical transactivation domain, a slightly shortened bZIP domain and a unique N-terminal sequence immediately upstream of the bZIP domain (20–22,30). We asked if Xv1s acts as an active transcription factor. Immunofluorescence revealed that ectopically expressed Xv1s was localized in both the cytoplasm and the nucleus, whereas Xv1u was mainly detected in the cytoplasm in HeLa cells (Fig. 2C). Subcellular fractionation of BT474 cells showed similar subcellular localization of endogenous Xv1s protein (Fig. 2D).

The nuclear localization of Xv1s supported a potential role as a transcription factor. We, therefore, determined the effects of Xv1s overexpression on gene transcription by RNA sequencing (RNA-seq) in HeLa cells. Gene set enrichment analysis (31,32) showed that multiple biological processes were significantly affected by Xv1s overexpression (Fig. 2E). However, the UPR was not affected, indicating that Xv1s does not regulate the canonical UPR. To confirm the differential activities of XBP1s and Xv1s, we transiently expressed Xv1s and XBP1s in BT474 and MCF7ca cells and examined the expression of XBP1s target genes, including DNAJC3, DNAJB9, BiP and HERP1 (33). As reported, XBP1s overexpression upregulated its target genes, whereas Xv1s overexpression had no effect on these UPR responsive genes (Fig. 2F). These results suggest that Xv1s is a transcription factor that does not regulate the canonical UPR.

Xv1s upregulates the polyglutamylase TTLL6

Further analysis of the RNA-seq dataset found that TTLL6 is one of the top-upregulated genes by Xv1s (Fig. 3A). RT-PCR confirmed TTLL6 mRNA upregulation in HeLa cells overexpressing Xv1s (Fig. 3B). Consistently, knockdown of Xv1 but not XBP1 markedly decreased TTLL6 mRNA levels (Fig. 3C). We next asked whether TTLL6 acts downstream of Xv1s in promoting cancer cell survival. TTLL6 siRNAs were transfected in BT474 cells and the benign MCF10A cells were used as a control. Like Xv1, TTLL6 knockdown caused apoptosis of BT474 cells as indicated by caspase 3/7 activation but not in non-cancerous MCF10A cells (Fig. 3D–F). TTLL6 siRNA transfection-induced apoptosis of BT474 cells was rescued by transient transfection of siRNA-resistant TTLL6 cDNA (Fig. 3G and H), suggesting that the siRNA specifically targeted TTLL6. Importantly, transient transfection of TTLL6 cDNA partially rescued BT474 cell death induced by Xv1 knockdown as evidenced by decreased caspase 3/7 activity (Fig. 3I and J). These results suggest that TTLL6 is a downstream effector of Xv1 function in cancer cell survival.

We then asked whether Xv1s directly binds to TTLL6 promoter and controls TTLL6 expression. Different regions of the putative promoter of TTLL6 were cloned and electrophoretic mobility shift assay (EMSA) was performed to identify the Xv1s binding region (34) (Fig. 4A**)**. An ~0.6 kb region (F5) that is localized in the putative promoter region is sufficient for Xv1s binding (Fig. 4A and B and Supplementary Material, Fig. S3). A luciferase reporter under the control of this promoter region was stably expressed in MCF7ca cells (Fig. 4C). Knockdown of Xv1 but not XBP1 significantly decreased the reporter activity (Fig. 4D), suggesting that the promoter region F5 contains the response element for Xv1s. Chromatin immunoprecipitation (ChIP)-quantitative PCR (qPCR) was used to determine Xv1s binding to the TTLL6 promoter in cells. Two fragments in the promoter region F5, designated as regions C and D, were enriched more than 10-fold by ectopically expressed Xv1s as compared with the control (Fig. 4E and F). The same sequences were not significantly enriched by XBP1s ectopic expression (Fig. 4E and F). EMSA confirmed that both C and D contained Xv1s binding sites (Fig. 4G). Consistently, the promotor region F5 efficiently drove a luciferase reporter expression, deletion of C and D from

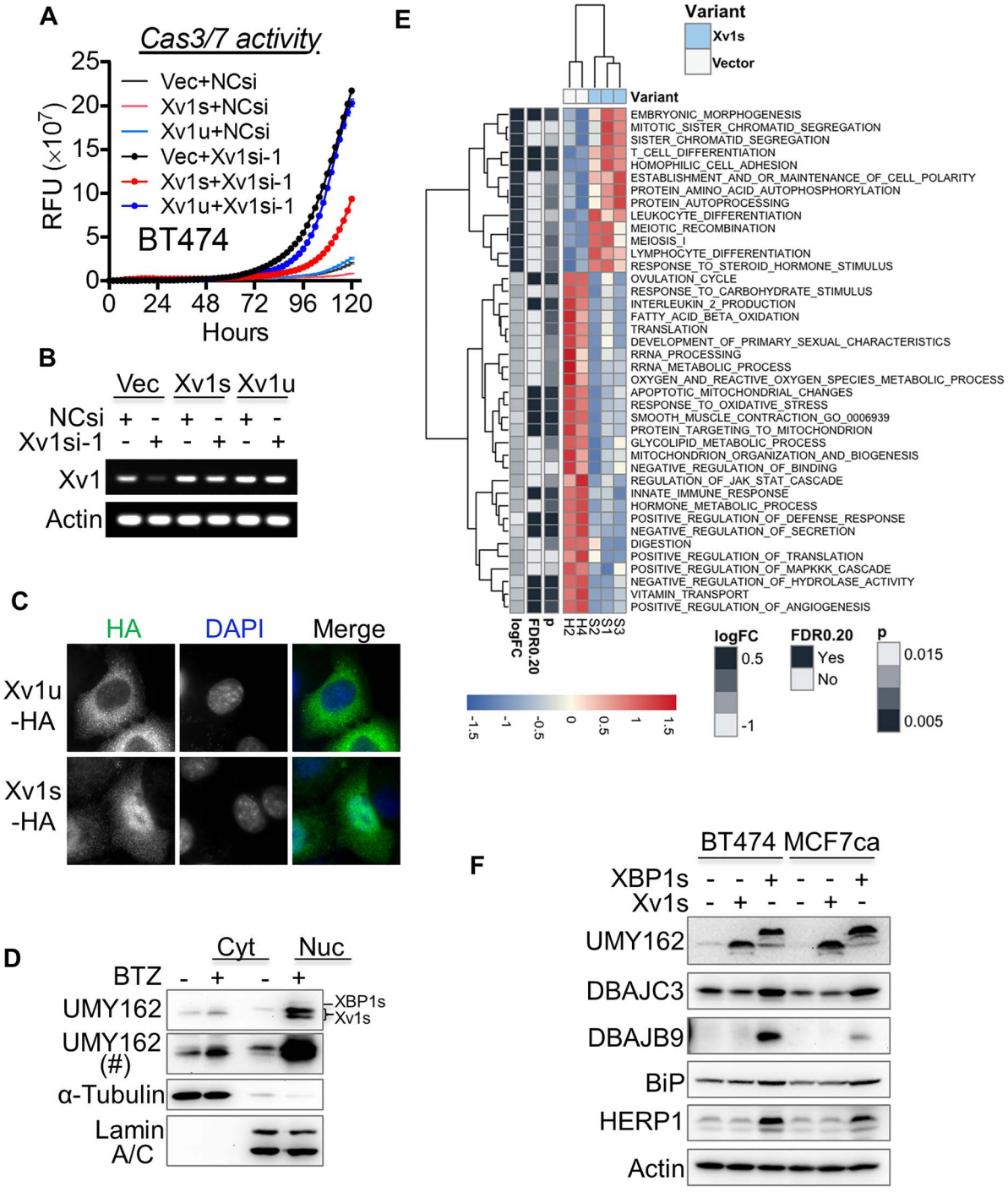

Figure 2. Xv1s is an active transcription factor that does not regulate the canonical UPR. (**A**) Xv1s rescues the effect of Xv1 RNAi. BT474 cells were first transfected with plasmids and then received a second transfection with siRNAs as indicated. Caspase 3/7 activities were monitored in live cells. $n = 12$ independent fields per condition. Data are means ± SEM for all graphs. (**B**) RT-PCR for A. (**C**) Immunofluorescence staining of HeLa cells transfected with HA-tagged Xv1u or Xv1s. (**D**) Nuclear cytoplasmic fractionation of BT474 cells treated with DMSO or BTZ (2 μM) for 2 h. Tubulin and Lamin A/C were blotted as cytoplasmic and nuclear markers, respectively. (**E**) Biological processes regulated by Xv1s in HeLa cells. RNA-seq datasets obtained from HeLa cells transfected with Xv1s cDNA and vector control were analyzed using Gene Set Enrichment Analysis software and Molecular Signature Database (MSigDB). (**F**) Xv1s does not affect the expression of the known XBP1s target genes. BT474 and MCF7ca cells transfected with Xv1s or XBP1s were analyzed for expression of XBP1 target genes, including DNAJC3, DNAJB9, BiP and HERP1.

F5 (F5AB) dramatically decreased the activity (Fig. 4H). Moreover, F5-driven siRNA-resistant TTLL6 expression efficiently rescued BT474 cells from apoptosis caused by TTLL6 RNAi, whereas F5AB failed to rescue the effects and also did not express TTLL6 (Fig. 4I and J). These data suggest that Xv1s binds to the TTLL6 promoter and transcribes TTLL6 gene, which further supports Xv1s as a transcription factor.

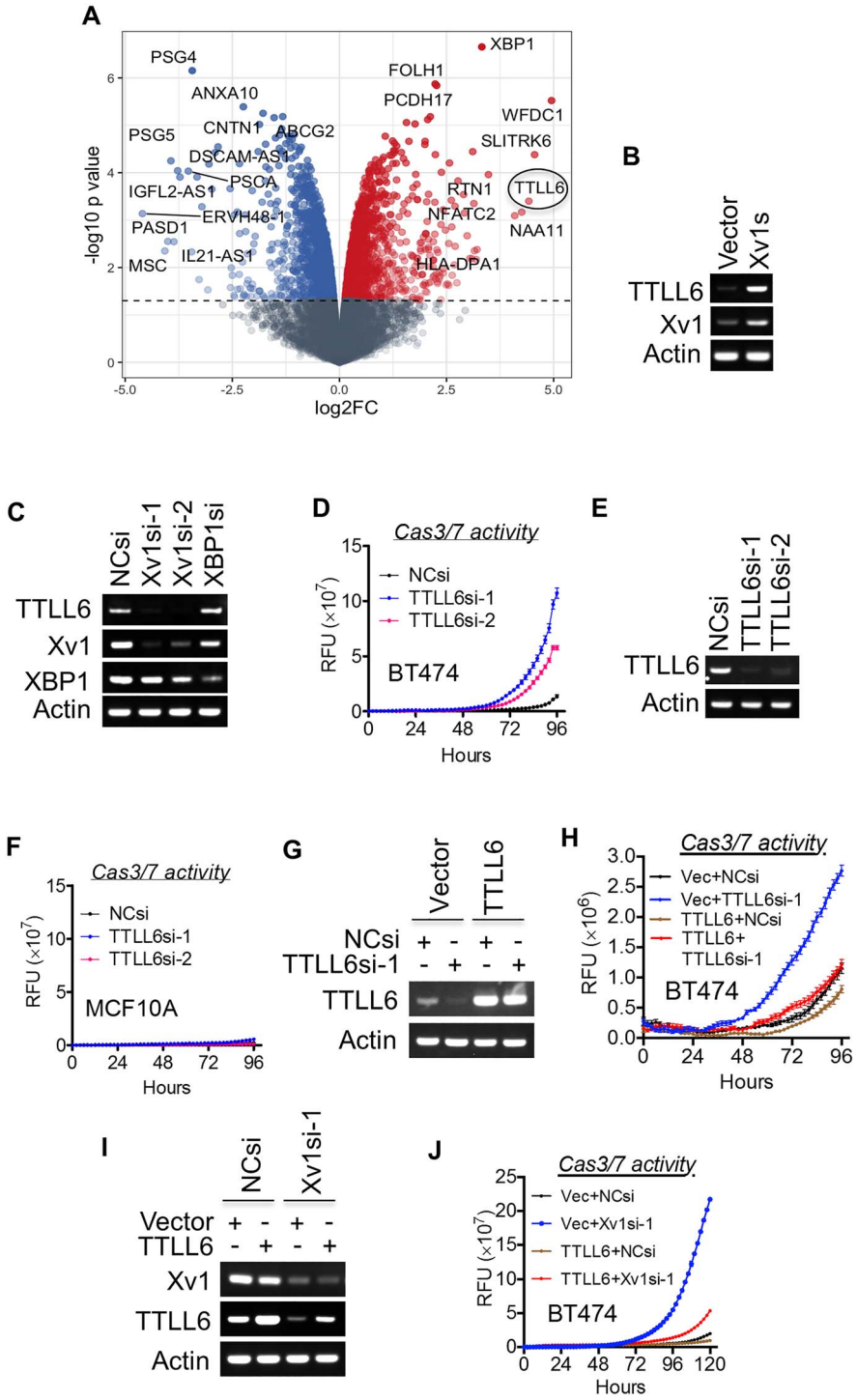

Figure 3. Xv1 mediates cancer cell survival through upregulation of TTLL6 expression. (**A**) Volcano plot of RNA-seq dataset obtained from HeLa cells transfected with Xv1s cDNA or vector control (Xv1s vs. vector). (**B**) RT-PCR of TTLL6 in HeLa transfected with vector or Xv1s cDNA. (**C**) RT-PCR of TTLL6 in BT474 cells transfected with indicated siRNAs. (**D** and **E**) Caspase 3/7 activity in live BT474 cells transfected with TTLL6 siRNAs. The knockdown efficiencies were detected by RT-PCR (E). $n = 12$ independent fields per condition. (**F**) Caspase 3/7 activity in live MCF10A cells transfected with TTLL6 siRNAs. $n = 12$ independent fields per condition. (**G** and **H**) siRNA-resistant TTLL6 cDNA rescues the effect of TTLL6 RNAi. BT474 cells were first transfected with plasmids and then received a second transfection with siRNAs as indicated. Caspase 3/7 activities were monitored in live cells. TTLL6 levels were detected by RT-PCR (H). $n = 12$ independent fields per condition. (**I** and **J**) TTLL6 rescues Xv1 knockdown-induced death of BT474 cells. BT474 cells were first transfected with vector or TTLL6 cDNA and then received a second transfection with siRNAs as indicated. Caspase 3/7 activities were monitored as aforementioned (I). TTLL6 and Xv1 levels were detected by RT-PCR (J). $n = 12$ independent fields per condition. Data are means ± SEM for all graphs.

Previous studies showed that overexpression of TTLL6 induces MT polyglutamylation and promotes MT severing in interphase HeLa cells (8). By immunofluorescence, we found that TTLL6 was also enriched in interpolar spindle and possibly also kinetochore MTs of mitotic BT474 cells (Fig. 5A), which coincides well with the reported pattern of spindle glutamylation (35). Immunofluorescent staining of HeLa cells

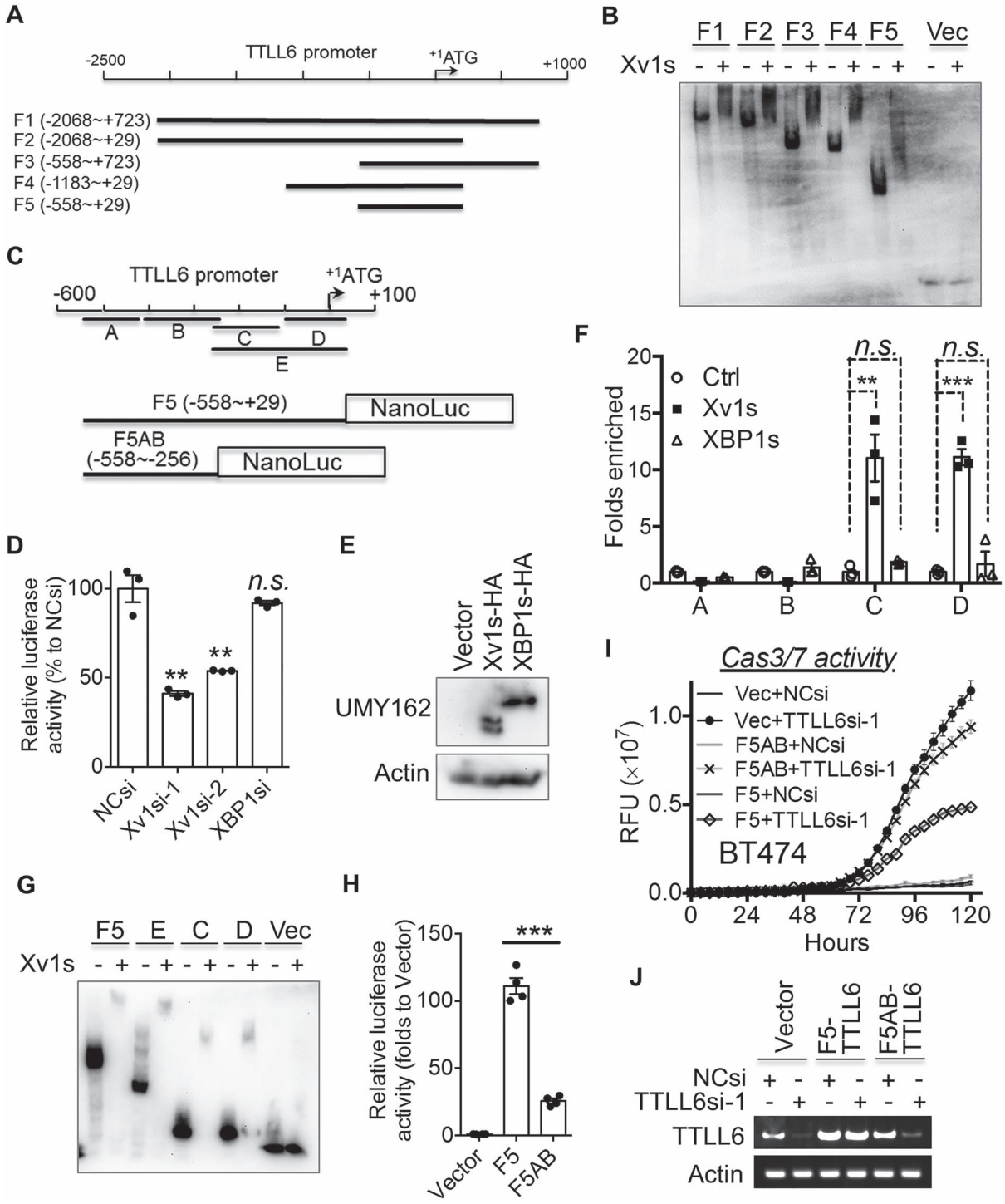

Figure 4. Xv1 mediates cancer cell survival through upregulation of TTLL6 expression. (**A**) Schematic of TTLL6 promoter. (**B**) EMSA. Probes used were shown in A. (**C**) Schematic of TTLL6 promoter reporters. (**D**) TTLL6 promoter reporter assay. MCF7ca cells stably expressing NanoLuc driven by TTLL6 promoter region F5 were transfected with siRNA as indicated. NanoLuc activity was measured from equal amount of proteins for each sample 48 h after transfection. The relative luciferase activity of each sample was plotted as percentage to negative control siRNA (NCsi)-transfected sample, by comparing their luminescent units. $n = 3$. Unpaired *t*-test for each sample versus NCsi control. (**E** and **F**) ChIP-qPCR. ChIP was performed using HeLa cells expressing vector control or HA-tagged Xv1s or XBP1s. Xv1s-HA and XBP1s-HA expression levels were shown by immunoblotting of the chromatins (E). The enrichment of each TTLL6 promoter fragment indicated in C was measured by qPCR (F). $n = 3$. Unpaired *t*-test. (**G**) EMSA. Probes used were shown in C. (**H**) TTLL6 promoter reporter assay. BT474 cells were transfected with vector or TTLL6 promoter reporters as indicated in C. NanoLuc (luciferase) activity was measured from equal amount of proteins for each sample 24 h after transfection. The relative luciferase activity of each sample was plotted as folds to vector transfected sample, by comparing their luminescent units. $n = 4$. Unpaired *t*-test. (**I** and **J**) Rescue of cell viability in BT474 cells knockdown of TTLL6 by siRNA-resistant TTLL6 cDNA driven by different TTLL6 promoter fragments. siRNA-resistant TTLL6 cDNA was expressed in BT474 cells under the control of TTLL6 promoter region F5 or F5AB that deleted the Xv1 binding regions C and D. Then the cells were transfected with negative control siRNA or TTLL6si-1 siRNA as indicated. Caspase 3/7 activities were monitored in live cells (I). TTLL6 levels were detected by RT-PCR (J). $n = 12$ independent fields per condition. Data are means ± SEM for all graphs. n.s., not significant; **, $P < 0.01$; ***, $P < 0.001$.

with overexpressing mCherry-TTLL6 or knocking down TTLL6 validated the specificity of the anti-TTLL6 antibody (Supplementary Material, Fig. S4). Importantly, knockdown of TTLL6 caused reduction of inter spindle MTs and unsuccessful chromosome congression (Fig. 5A), which was accompanied by decreases in polyglutamylation of both total MTs and spindle MTs (Fig. 5B–E). In agreement with our observation that TTLL6 acts a downstream effector of Xv1, Xv1 knockdown almost phenocopied the effect of TTLL6 knockdown, whereas XBP1 knockdown showed no effect (Fig. 5B–E). Xv1 or TTLL6 knockdown did not affect the length and width of mitotic spindle (Fig. 5F and G). These results suggest that Xv1-mediated TTLL6 expression plays an important role in mitosis. To obtain further support, we assessed the mitotic index in BT474 and MCF7ca cells 48 h after Xv1 or TTLL6 siRNA knockdown, a timepoint when minimal apoptosis has been activated (22). Normal human retinal pigment epithelial-1 (RPE1) cells were used as a control. Knockdown of XBP1 was performed for comparison. The results showed that knockdown of either TTLL6 or Xv1 increases mitotic index by about 3- to 5-fold as compared with control knockdown, whereas XBP1 knockdown cells had no effect (Fig. 5H and Supplementary Material, Fig. S5). RPE1 cells did not express either Xv1 or TTLL6 (Supplementary Material, Fig. S6A). Transfection of siRNAs targeting Xv1, TTLL6 or XBP1 did not affect mitosis of RPE1 cells (Fig. 5H and Supplementary Material, Fig. S6B and C). In addition, knockdown of Xv1 or TTLL6 arrested mitosis mainly at prometaphase and metaphase in both BT474 and MCF7ca cells with misaligned chromosomes in 55–60% mitotic cells (Fig. 5I–K). Knockdown of XBP1 had no effects on mitosis (Fig. 5I–K). Notably, knockdown of Xv1 or TTLL6 had no effect on tubulin detyrosination (Supplementary Material, Fig. S7). These results suggest that Xv1 is required for successful completion of mitosis of cancer cells, which is mediated, at least in part, by upregulation of TTLL6 to catalyze polyglutamylation of spindle MTs.

Downregulation of TTLL6 by RNAi correlates with decreases in spindle polyglutamylation and interpolar MTs (Fig. 5A–E). This result is consistent with previous reports that polyglutamylation stabilizes MTs and increases MT mass by promoting GTP-tubulin incorporation (36,37). Thus, loss of polyglutamylation in Xv1 and TTLL6 knockdown cells would decrease spindle mass. Consistently, we observed that the end-binding protein 1 (EB1) that preferentially binds to the growing ends of MTs by sensing GTP-tubulin (38–40) colocalized with spindle MTs with a clear concentration at the plus ends (around the spindle equator) in control and XBP1 knockdown cells (Fig. 6A). In contrast, the EB1 localization to spindle markedly decreased in Xv1 and TTLL6 knockdown cells compared with control cells (Fig. 6A and B).

The reduction in spindle MT polyglutamylation in Xv1 and TTLL6 knockdown cells led us to examine its acetylation, because it has been postulated that polyglutamylation may facilitate acetylation of MTs (41). In support of this possibility, we demonstrated a drastic decrease in spindle MT acetylation in both Xv1 and TTLL6 knockdown cells (Fig. 6C and D). To determine the cause for the misalignment of chromosomes in Xv1 and TTLL6 knockdown cells, we examined the stability of kinetochore fibers (k-fibers). It is known that k-fibers are depolymerized in cold-treated cells when not stably end-on attached to kinetochores (42). The results showed that cold-resistant k-fibers were disorganized and some chromosomes were not attached to k-fibers in Xv1 and TTLL6 knockdown cells, as revealed by examining colocalization of cold-resistant k-fibers and kinetochores labeled by α-tubulin antibody and the anti-centromere antibodies (ACAs), respectively (Fig. 6E). Thus, the failure in MT attachment to kinetochore may cause failure in chromosomal congression. Together, these data suggest a key role of the Xv1 in spindle MT polyglutamylation and acetylation, and in maintaining spindle structure, dynamics and chromosome-kinetochore attachment, which is, at least in part, mediated by TTLL6. Loss of function of the Xv1 and TTLL6 impairs mitosis, leading to cancer cell death.

Discussion

We have previously reported that Xv1 is highly enriched in cancer tissues and is specifically required for survival of a variety of cancer cells (22). We have now identified a novel IRE1β-Xv1-TTLL6 pathway that specifically regulates mitosis of cancer cells. Loss of cell cycle control is a hallmark of cancer and has been a proven drug target for cancer therapy for decades. However, the current cell cycle-targeted drugs in general have a low therapeutic index because of severe toxicity to normal cells (43,44). Therefore, strategies that target cell cycle features that are distinct to cancer cells are desirable (43,44). These features are likely regulated by genes or gene variants that are enriched or specifically expressed in cancer cells (43–46). Discovery of the IRE1β-Xv1-TTLL6 pathway that operates specifically in cancer cells to promote mitosis may provide new opportunities to develop cancer selective anti-mitosis drugs that could overcome the low therapeutic index of the pan-acting drugs. In addition, the elevated expression of Xv1 could serve as a pharmacogenetic biomarker for drugs that target this novel pathway.

Like XBP1, Xv1 activation also starts with unconventional splicing of its mRNA (Fig. 1). Both XBP1 and Xv1 mRNAs are spliced by IRE1α under ER stress, but our data support that Xv1 mRNA is also constitutively spliced by IRE1β. This is consistent with previous reports that IRE1β is constitutively active in cells (28,47). Although IRE1β has been shown to regulate airway mucin production through splicing XBP1 mRNA (48), most studies reported that IRE1β shows minimal RNase activity toward XBP1 (26,49–51) and is not involved in UPR (52). Moreover, IRE1β has been shown to assemble with IRE1α and inhibit IRE1α-mediated XBP1 splicing under ER stress (51). Elements in XBP1u mRNA and protein that are

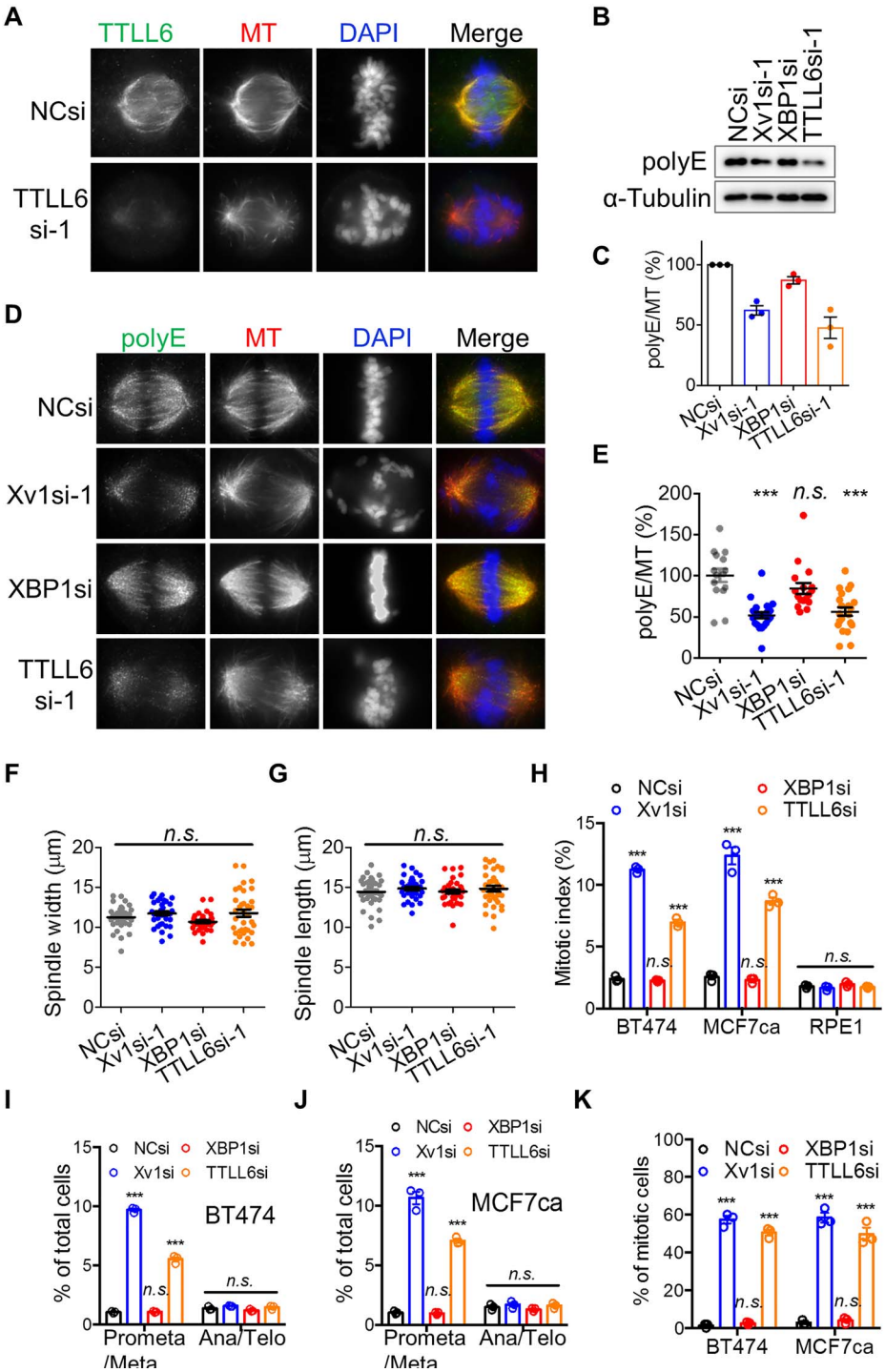

Figure 5. Knockdown of Xv1 or TTLL6 decreases polyglutamylation of MT and induces mitotic arrest in cancer cells. (**A**) Knockdown of TTLL6 causes spindle disorganization. MTs were stained with a α-tubulin antibody. (**B** and **C**) Knockdown of Xv1 or TTLL6 decreases MT polyglutamylation. Total MTs were isolated from BT474 cells transfected with different siRNA as indicated and processed for immunoblotting (B). Band density of polyE was normalized to that of α-tubulin and plotted (C). $n = 3$ experiments. (**D** and **E**) Knockdown of Xv1 or TTLL6 decreases polyglutamylation on spindles. BT474 cells transfected with different siRNA as indicated were immunostained for polyE and MT (D). The immunofluorescence intensities of polyE were quantified and normalized to MT staining (E). $n = 15$ (NCsi), $n = 21$ (Xv1si-1), $n = 17$ (XBP1si), $n = 21$ (TTLL6si-1) spindles. (**F** and **G**) Knockdown of Xv1 or TTLL6 does not affect spindle size. BT474 cells transfected with different siRNA as indicated were immunostained for MT. The length (F) and width (G) of the spindles in prometaphase/metaphase cells were measured by Image J. $n = 35$ (NCsi), $n = 35$ (Xv1si-1), $n = 32$ (XBP1si), $n = 35$ (TTLL6si-1) spindles. (**H**) Mitotic index. BT474, MCF7ca or RPE1 cells were transfected with different siRNA as indicated. Two days after siRNA transfection, mitotic cells and total cells were counted on the basis of the DNA and MT staining. $n = 3$ replicates. (**I** and **J**) Knockdown of Xv1 or TTLL6 arrests cells mainly at prometaphase/metaphase in BT474 (I) and MCF7ca (J) cells. Mitotic cells were counted as in H and grouped into two groups: prometaphase and metaphase (Prometa/Meta), and anaphase and telophase (Ana/Telo). $n = 3$ replicates. (**K**) Knockdown of Xv1 or TTLL6 induces chromosome misalignment in BT474 and MCF7ca cells. Cells containing misaligned chromosomes and total mitotic cells were counted as in H. $n = 3$ replicates. Unpaired *t*-test for each sample versus NCsi control in each group. n.s., not significant; ***, $P < 0.001$. Data are means ± SEM for all graphs.

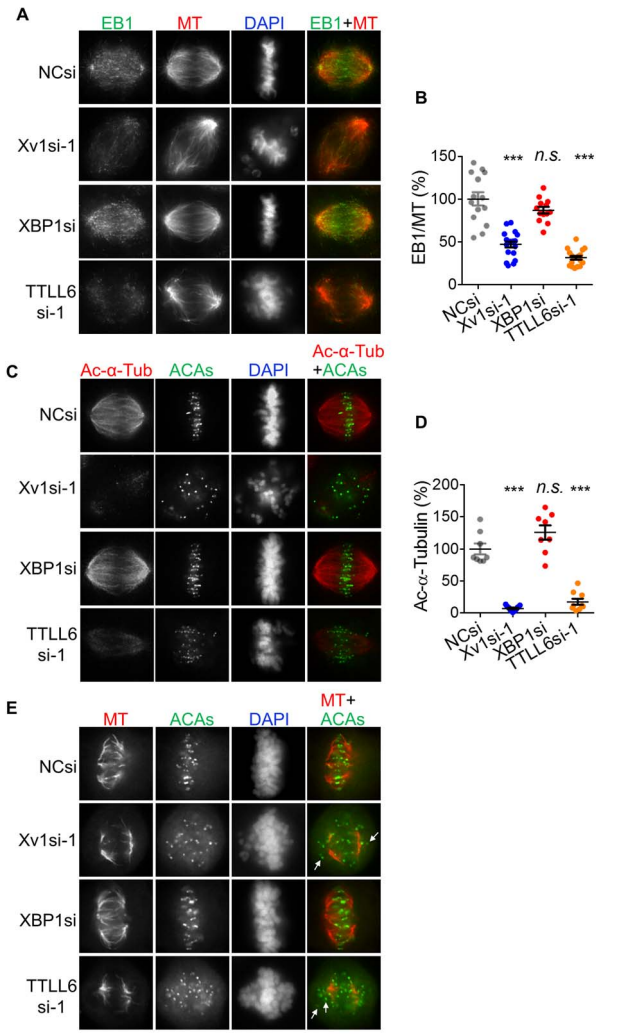

Figure 6. Knockdown of Xv1 or TTLL6 causes spindle defects. (**A** and **B**) Knockdown of Xv1 or TTLL6 decreases EB1 binding on spindles. BT474 cells transfected with different siRNA as indicated were immunostained for EB1 and MT (A). The immunofluorescence intensities of EB1 were quantified and normalized to MT staining (B). $n = 14$ (NCsi), $n = 18$ (Xv1si-1), $n = 13$ (XBP1si), $n = 18$ (TTLL6si-1) spindles. (**C** and **D**) Knockdown of Xv1 or TTLL6 decreases acetylation on spindles in BT474 cells. Ac-α-Tub, acetyl-α-tubulin. ACAs were costained to identify the kinetochore. $n = 8$ (NCsi), $n = 13$ (Xv1si-1), $n = 8$ (XBP1si), $n = 9$ (TTLL6si-1) spindles. (**E**) Knockdown of Xv1 or TTLL6 decreases kinetochore attachment with cold-resistant spindle MTs in BT474 cells. Cells were cold-treated before fixation. Arrows indicate the kinetochores that are not attached to cold-resistant MTs. Data are means ± SEM for all graphs. Unpaired *t*-test for each sample versus NCsi control. n.s., not significant; ***, $P < 0.001$.

required for splicing by IRE1α are also found in Xv1u mRNA and protein (53–56). Thus, it is not surprising that both Xv1 and XBP1 mRNAs are spliced by IRE1α. Why IRE1β preferentially splices Xv1 mRNA is not known. The unique 5′ mRNA sequence and/or the novel N-terminus of Xv1 protein may render the preferential splicing. Further studies are required to address this issue.

Unlike XBP1s, Xv1s does not regulate the canonical UPR, suggesting that the shorter bZiP domain and the different N-terminal sequence in Xv1s may alter its DNA binding preference. Using EMSA and ChIP-qPCR, we confirmed that Xv1s and XBP1s have different DNA binding preferences and mapped Xv1s binding sites to two small regions in the TTLL6 promoter (Fig. 4). In contrast, XBP1s binding motifs were not identified in the two TTLL6 promotor regions, suggesting that the binding motif of Xv1s is different from that of XBP1s. In addition, our data suggest that overexpressed Xv1s is phosphorylated at Ser162 and the phosphorylated Xv1s is localized in the nucleus (Fig. 2B and C and Supplementary Material, Fig. S1). This result raises interesting possibilities that the phosphorylation may regulate Xv1s transcriptional activity by affecting its interaction with other transcriptional regulators, binding to DNA and/or nuclear import.

The polyglutamylase TTLL6 was identified as a top-upregulated gene by Xv1s (Fig. 3A–C). We showed that it is localized in mitotic spindle (Fig. 5A). Knockdown of TTLL6 or its upstream regulator Xv1s decreases spindle polyglutamylation and interpolar MTs, impairs chromosome alignment and causes mitotic arrest and cell death of breast cancer BT474 cells (Figs 3C and D and 5H–J). In the non-cancerous breast epithelial cell MCF10A that does not require Xv1 (22), knockdown of TTLL6 did not affect cell viability (Fig. 3). The same results were observed in human normal eye pigment epithelial-1 (RPE1) cells (Fig. 5H and Supplementary Material, Fig. S6). These results support a function of the Xv1-TTLL6 pathway in mitosis that is unique to cancer cells.

The spindle defects caused by Xv1 knockdown are likely the consequence of decrease in MT polyglutamylation. Previous studies have reported a role of MT polyglutamylation in cancer cell mitosis (35,57). Tubulin glutamylation increases during mitosis and the increase appears more obvious in pole-to-pole and kinetochore MTs in HeLa cells (35). Microinjection of anti-polyglutamylated tubulin antibody GT335 in G2 phase HeLa cells caused centrosome fragmentation and multipolar spindle (57). However, the lack of knowledge about the regulation of this tubulin modification during mitosis precluded a complete understanding of its functional significance. We have now demonstrated that Xv1s transcribes TTLL6 that in turn promotes mitosis of cancer cells. All cancer cells and the benign MCF10A cells but not the normal RPE1 cells tested in this study express variable levels of TTLL6; why cancer cells are more dependent on this protein for mitosis is not well understood. We speculate that Xv1s may also regulate other protein(s) that acts together with TTLL6 to enhance mitosis of cancer cells. Furthermore, it is conceivable that non-cancerous cells have distinct upstream regulators of TTLL6 transcription than cancer cells.

The decrease in polyglutamylation of mitotic spindle is likely the central cause for the reduction of interpolar spindle we have observed in Xv1 and TTLL6 knockdown cancer cells. Previous studies have reported that polyglutamylation stabilizes MTs and increases MT mass (36,37). Polyglutamylation activates MT severing enzymes, such as spastin and katanin (8,36,58–60). Severing of MTs creates nanoscale damages throughout the MT by active extraction of tubulin heterodimers (36). These damage

sites are repaired spontaneously by GTP-tubulin incorporation, which rejuvenates and stabilizes MTs, leading to increases in MT mass (36,37). Thus, loss of polyglutamylation in Xv1 and TTLL6 knockdown cells would diminish severing enzyme-dependent repair and stabilization, leading to decreases in interpolar spindle mass (Figs 5 and 6). In support of this possibility, the localization of the EB1 that preferentially binds to the growing MT ends by sensing GTP-tubulin (38–40) to spindle, markedly decreased in Xv1 and TTLL6 knockdown cells compared with control cells (Fig. 6A and B). Acetylation of α-tubulin by tubulin acetyltransferase aTAT1 takes place only in the lumen of MTs (61–64). aTAT1 may enter the lumen of MTs through the damage sites created by polyglutamylation-dependent severing (41). In support of this possibility, we demonstrated a drastic decrease in spindle MT acetylation in both Xv1 and TTLL6 knockdown cells (Fig. 6C and D). Our data suggest that polyglutamylation also regulates kinetochore fibers (k-fibers) attachment to kinetochore. It is known that k-fibers are depolymerized in cold-treated cells when not stably end-on attached to kinetochores (42,65). We found that cold-resistant k-fibers were reduced, disorganized and some chromosomes were not attached to k-fibers in Xv1 and TTLL6 knockdown cells (Fig. 6E). Together, our results suggest a key role of spindle polyglutamylation regulated by the Xv1-TTLL6 pathway in maintaining spindle structure, dynamics and acetylation all of which are involved in mitotic progression of cancer cells.

Although the effects of Xv1s on MT polyglutamylation were apparent, we cannot exclude the possibility that Xv1s and TTLL6 may also regulate mitosis through additional mechanisms. Previous studies have reported that TTLL6 catalyzes cGAS polyglutamylation, which inhibits its DNA binding and represses the innate immune response to viral infections (1,18). TTLL6 also catalyzes Mad2 polyglutamylation, which plays a critical role in megakaryopoiesis (19). How cGAS and Mad2 polyglutamylation might be involved in mitosis regulation warrants future investigation. Although the mechanisms of the downstream events of Xv1 and TTL6 are not completely understood, mitotic arrest-induced mitotic catastrophe and cGAS activation are the likely causes of cancer cell death when the Xv1-TTLL6 pathway is disrupted (66), (67).

Materials and Methods

Cell culture

HeLa, U251, U2OS, HepG2, MCF10A, RPE1 and BT474 cell lines were purchased from ATCC. MCF7ca (MCF7 human breast cancer cells transfected with aromatase gene) cells were obtained from Dr Yun Qiu (University of Maryland, Baltimore).

All cell lines were grown at 37°C with 5% CO_2. MCF10A cells were maintained in Dulbecco's Modified Eagle's medium (DMEM)/F12 supplemented with 5% horse serum, human epidermal growth factor (20 ng/ml), hydrocortisone (500 μg/ml), insulin (10 μg/ml), cholera toxin (100 ng/ml). Other cell lines were maintained in DMEM supplemented with 10% fetal bovine serum.

Antibodies

Horseradish peroxidase (HRP)-conjugated streptavidin (#3999) and antibody to α-tubulin (DM1A, #3873) were purchased from Cell Signaling Technology. Antibody to DNAJB9 (13157–1-AP) and HRP-conjugated α-tubulin antibody (HRP-66031) were purchased from Proteintech. Antibody to acetylated α-tubulin (sc-23 950) was purchased from Santa Cruz Biotechnology. Anti-β-actin-peroxidase antibody (A3854), anti-tyrosinated α-tubulin antibody (MAB1864–1), anti-detyrosinated α-tubulin antibody (AB3201), anti-Lamin A/C antibody (SAB4200236) and TTLL6 antibody (HPA052397) were purchased from Sigma. Anti-centromere antibodies (15–235) were purchased from Antibodies Incorporated. Anti-polyglutamate chain (polyE) antibodies (AG-25B-0030) were purchased from Adipogen. EB1 antibody (ab53358) was purchased from Abcam. HERP1 antibody (TA507019) was purchased from Origene. BiP antibody (610978) was purchased from BD Transduction Laboratories. DNAJC3 antibody (MA5–14820) was purchased from Invitrogen. Anti-HA (3F10) antibody (11867423001) was purchased from Roche. Ire1β antibody (MBS9210486) was purchased from MyBioSource. HRP or Alexa Fluor dye-conjugated secondary antibodies were all purchased from Invitrogen.

To produce antibodies (UMY162) that can recognize all XBP1u/s and Xv1u/s proteins, a common peptide of these proteins (RQRLGMDALVAEEEAEAC) was synthesized by Peptide 2.0 Inc. (Chantilly, VA). A cysteine was added to the C-terminus for conjugation of the peptide to keyhole limpet hemocyanin to improve the immunogenicity. UMY162 was purified from rabbit antiserum using the same peptide that was biotinylated at the C-terminus and bound to streptavidin magnetic beads (Thermo Scientific, Waltham, MA).

Plasmid constructs

Xv1 cDNA with a HA-tag coding sequence fused to the 3′ end of Xv1s open reading frame (ORF) was synthesized by Gene Universal Inc. and subcloned into pLVX-EF1α-IRES-puro (Clontech). To express XBP1 and TTLL6, XBP1 and TTLL6 cDNAs were amplified by RT-PCR from U251 cDNA and cloned into pLVX-EF1α-IRES-puro. To make pLVX-XBP1s-HA and pLVX-Xv1s-HA, the 26-base pair intron sequence was removed by Q5 site-directed mutagenesis kit (New England Biolabs). pLVX-Xv1u-HA were constructed by PCR. To make pLVX-Xv1u-HA that cannot be spliced by IRE1, two silent mutations were made by QuickChange II site-directed mutagenesis kit (Agilent) in IRE1 recognition sites, which breaks the stem-loop structure for IRE1 recognition (68). For Xv1 RNAi rescue experiments, plasmids harboring Xv1 siRNA (Xv1si)-resistant Xv1s-HA or Xv1u-HA cDNAs were made by

site-directed mutagenesis. Two nucleotides in Xv1si-1-targeting site were changed. Similarly, TTLL6si-1 siRNA-resistant TTLL6 cDNA was made by site-directed mutagenesis. TTLL6 promoter fragments were PCR amplified from HeLa cell genomic DNA and inserted into pNL1.1 for EMSA and promoter assay. To express TTLL6si-1 siRNA-resistant TTLL6 under the control of TTLL6 promoter fragment F5 or F5AB that deleted regions C and D, the original EF1α promoter that drives TTLL6 expression was replaced by F5 or F5AB, respectively. All constructs and mutations were verified by DNA sequencing. All primers used are listed in Supplementary Material, Table S1.

RT-PCR

Total RNA was prepared using Trizol reagent (Invitrogen) according to the manufacturer's protocol. Reverse transcription was performed using ProtoScript® First Strand cDNA Synthesis kit (New England BioLabs) using 2 μg total RNA/reaction. Primers used in RT-PCR are listed in Supplementary Material, Table S1.

RNA-seq

HeLa cells were transfected with vector or pLVX-Xv1s by Lipofectamine 2000 (Invitrogen). Two days after transfection, total RNA was prepared from these cells using Trizol reagent (Invitrogen) according to the manufacturer's protocol. The RNA samples were sent to Novogene Corporation Inc. for quality control and RNA-seq services. Skewer was used to trim adapters from paired end reads, and HISAT2 was used to align sequences to *Homo sapiens* National Center for Biotechnology Information reference genome assembly version GRCh38 (69–71). The align reads were counted and assigned gene features using featureCounts as a part of the Subread package (71). Analysis of counts was conducted using the R programming language and Bioconductor libraries including edgeR, limma and gene set variation analysis (GSVA) (31,72,73). After counts were transformed and normalized, preprocessing for modeling was conducted using the voom-limma procedure before differential expression analysis. GSVA enrichment was performed with MSigDB defined gene sets (31,32).

RNA interference

Negative control #1 siRNA was purchased from Ambion. All other siRNAs were synthesized by Sigma, including Xv1si-1 (sense: 5′-CCUCUUAACUCGGACAUGAdTdT-3′), Xv1si-2 (sense: 5'-CUCUCGUUAGAGAUGACCAdTdT-3′), XBP1si (sense: 5'-GACCCCUAAAGUUCUGCUUdTdT-3′), TTLL6si-1 (sense: 5'-GAAACGUAUGAGAAGGAAAdTdT-3′), TTLL6si-2 (sense: 5'-GCUUUGCGACGACCUCUUAdTdT-3′), IRE1βsi (sense: 5'-GGGAUUAAUGAAACUGCCAdTdT-3′). Lipofectamine RNAiMAX (Invitrogen) was used to transfect siRNAs.

Database analysis

The relative expression levels of IRE1α and IRE1β in the transcriptomic datasets genotype-tissue expression (GTEx) and TCGA were analyzed using the TCGA TARGET GTEx study (74). GTEx has expression data from normal tissues, whereas TCGA contains the data from tumors and a limited number of normal tissues near the tumors.

Live cell analysis

Real-time apoptosis was monitored using an IncuCyte@ S3 Live-Cell Analysis System (Sartorius). Cells were seeded to 96-well plates. The next day, the culture medium was replaced with fresh one containing IncuCyte@ Caspase 3/7 Green reagent (1:2000 final), which generates green fluorescence once cleaved by activated caspase 3/7. The cells were then transfected with different siRNAs with Lipofectamine RNAiMAX. Green fluorescence was monitored by time-lapse imaging and normalized to real-time cell confluence. For rescue experiments, cells were first transfected with plasmids using X-tremeGENE HP DNA Transfection Reagent (Roche). Sixteen hours after transfection, the cells were seeded to 96-well plates and then followed the aforementioned protocol for siRNA transfection and caspase 3/7-activity monitoring.

Nuclear cytoplasmic fractionation

BT474 cells were treated with dimethyl sulfoxide (DMSO) or BTZ (2 μM) for 2 h. The nuclear and cytoplasmic fractions were prepared from these cells using NE-PER™ Nuclear and Cytoplasmic Extraction Reagents (Thermo) following the manufacturer's protocol.

TTLL6 promoter assay

TTLL6 promoter F5 reporter plasmid was cotransfected with pBABE-puro in 20:1 ratio into MCF7ca cells with Lipofectamine 2000 (Invitrogen). Twenty-four hours after transfection, the cells were selected with 6 μg/ml puromycin. NanoLuc (luciferase) activity of each stable clone was measured. The one that stably expressing TTLL6 promoter F5 reporter was used in the TTLL6 promoter assays. The cells were transfected with different siRNA as aforementioned. Forty-eight hours after transfection, the cells were lysed in NanoLuc assay buffer [100 mM MES pH 6.0, 1 mM CDTA, 0.5% (v/v) Tergitol, 0.05% (v/v) Mazu DF 204, 150 mM KCl, 1 mM DTT] (75). Equal amount of protein was used to measure NanoLuc activity with coelenterazine H (10 μM final).

EMSA

Different TTLL6 promoter regions were PCR amplified and clone into EcoR V site of pNL1.1. A set of biotin-labeled primers were used to amplify these promoter regions for EMSA. DNA fragment amplified from the empty vector was used as control. To express Hi-tagged Xv1s, cDNA of Xv1s was cloned to Nco I/Not I sites of pET28a. The protein was expressed in BL21(DE3) at room temperature by 0.5 mM isopropyl-β-D-1-thiogalactopyranoside (IPTG) induction for 2 h. Then the protein was purified using Ni-NTA (Qiagen) following the

manufacturer's manual following by dialysis against PBS. EMSA was performed using 10 nM biotin-labeled probe and 50 ng purified Xv1s in 100 mM Tris–HCl (pH 7.5), 100 mM NaCl, 2 mM $MgCl_2$, 50 mg/ml bovine serum albumin (BSA), 5% glycerol. The samples were separated in 5% native polyacrylamide gel in 0.5 × TBE. The biotin-labeled probes were detected with HRP-conjugated streptavidin.

ChIP-qPCR

ChIP was performed using SimpleChIP® Enzymatic Chromatin IP kit (Cell signaling technology) following the manufacturer's protocol. HeLa cells were transfected with empty vector or pLVX-Xv1s-HA or pLVX-XBP1s-HA for 24 h before cross-linking with 1% formaldehyde for 17 min at room temperature. Cross-linked chromatin preparation of each sample containing 8 μg DNA was used in ChIP. Anti-HA Affinity Matrix (Roche) that specifically recognizes HA-tag was pre-blocked in 500 μL of ChIP buffer containing 100 μg denatured herring sperm DNA and 100 μg BSA for 1 h at 4°C. The ChIP samples were incubated overnight at 4°C with rotation. After proteinase K digestion, DNA bound to the beads was purified and used in qPCR. A 2% input control for each sample was also used in qPCR. Four sets of primers were designed to amplify four different fragments in TTLL6 promoter region. To calculate the relative level for each fragment, the threshold cycle (Ct) value for ChIP sample was normalized to the value for 2% input control [ΔCt = Ct (ChIP)-Ct (2% input)]. The relative level was calculated as $2^{\Delta Ct}$ for each sample. Notably, the 2% input controls for each fragment had similar Ct values in all samples, confirming that equal amount of DNA was loaded in each ChIP. To calculate the enrichment of each fragment, the relative levels of Xv1s and XBP1 samples were normalized to that of empty vector control.

MT isolation

MT isolation was performed as previously reported (76), with some modifications. BT474 cells (~1 × 10^6) transfected with different siRNAs for 2 days were lysed in large volume (2 ml) of PEM buffer [100 mM 1.4-piperazine-bis-ethane sulfonic acid (PIPES), pH 6.9, 5 mM $MgCl_2$, 1 mM ethylene glycol tetraacetic acid (EGTA)] with 0.5% Triton X-100 and 10 μM paclitaxel for 10 min at 37°C. After centrifugation at 20 000 × g for 10 min, the supernatant containing free tubulin was removed. The pellet containing MTs was briefly washed with PEM buffer and then lysed directly in sampling buffer for immunoblotting.

Immunofluorescence

For better labeling efficiencies, different fixation conditions were applied to different primary antibodies. In all cases, Alexa Fluor 488 or 594-conjugated secondary antibodies were used to label the primary antibodies at room temperature for 1 h. Nuclei were labeled with DAPI. Fluorescent microscopy was performed using a Zeiss Axiovert 200 M fluorescent microscope.

To analyze the localization of Xv1s and Xv1u, HeLa cells growing on coverslips were transfected with pLVX-Xv1s-HA or pLVX-Xv1u-HA using Lipofectamine 2000. About 24 h after transfection, the cells were washed with PBS and fixed in 4% paraformaldehyde (PFA) for 30 min at room temperature. The cells were blocked in 3% BSA and then labeled with rat monoclonal anti-HA antibody (3F10, 1:1000).

To analyze the effects of knockdown Xv1 or TTLL6 on polyglutamylation of MT, BT474 cells transfected with different siRNAs for 2 days were fixed with an optimized method to better preserve MT structures (77). Briefly, the cells were prefixed in protein crosslinking reagent dithiobis (succinimidylpropionate) (DSP) for 10 min at 37°C. Then the cells were permeabilized with 0.5% Triton X-100 in MT-stabilizing buffer (MTSB, 1 mM EGTA, 4% PEG8000, 100 mM PIPES, pH 6.9) for 10 min at 37°C followed by fixation with 4% PFA in MTSB for 15 min at 37°C. After blocking in 5% goat serum in phosphate-buffered saline (PBS) for 1 h, the cells were labeled with rabbit polyE antibody (1:1000) and α-tubulin antibody (DM1A, 1:800) for overnight at 4°C. To label the localization of TTLL6, BT474 cells were fixed as for polyE staining. Rabbit polyclonal TTLL6 antibody (1:50) and mouse monoclonal α-tubulin antibody (DM1A, 1:800) were used to label TTLL6 and the MTs (MT) for overnight at 4°C. TTLL6 and detyrosinated-α-tubulin were labeled with rabbit polyclonal TTLL6 antibody (1:50) and detyrosinated-α-tubulin antibody (AB3201, 1:500), respectively.

For EB1 staining, BT474 cells transfected with different siRNAs for 2 days were also prefixed in DSP for 10 min at 37°C and then fixed in cold methanol for 10 min at −20°C. Rat monoclonal EB1 antibody (1:500) was costained with α-tubulin antibody (DM1A, 1:800) for overnight at 4°C.

To costain acetylated α-tubulin and kinetochore, BT474 cells transfected with different siRNAs for 2 days were fixed in 4% PFA in culture media for 20 min at 37°C. The cells were labeled with mouse monoclonal acetylated α-tubulin antibody (1:500) and anti-centromere antibodies [ACAs, 1:100) derived from human CREST syndrome (calcinosis, Raynaud phenomenon, esophageal dysmotility, sclerodactyly, and telangiectasia) patient serum] for overnight at 4°C.

To analyze cold stabilities of MTs in different knockdown cells, BT474 cells transfected with different siRNAs for 2 days were incubated in precooled PBS for 10 min on ice. Then the cells were fixed at room temperature for 10 min with 4% PFA in 100 mM PIPES pH 6.8, 10 mM EGTA, 1 mM $MgCl_2$, 0.2% Triton X-100 (78). ACAs and α-tubulin antibody (DM1A) were then used to label the kinetochores and MTs.

To analyze mitotic index, BT474, MCF7ca and RPE1 cells were transfected with different siRNAs for 2 days and then fixed with cold methanol for 20 min at −20°C. MT was labeled with α-tubulin antibody (DM1A, 1:800) and the nucleus was labeled with propidium iodide.

Statistical analysis

Statistical significance was assessed by paired or unpaired two-tailed Student's *t*-test using GraphPad Prism 7.0. For all analyses, $P > 0.05$ was considered not significant (ns), whereas $P \leq 0.05$ (*), $P \leq 0.01$ (**) and $P \leq 0.001$ (***) are considered statistically significant.

Supplementary Material

Supplementary Material is available at *HMG* online.

Acknowledgements

We thank Drs Jiaoti Huang and Alexander Kelly for valuable suggestions.

Conflict of Interest statement. A patent application detailing the findings in this manuscript have been filed by the University of Maryland, Baltimore. Patent number: WO/2021/119561. Patent title: Inhibitors of cancer biomarkers and uses thereof.

Funding

National Institutes of Health grant UO1GM117175 to S.F. G.R., D.Y.T., and M.J.H. were supported by the Intramural Research Program of the National Center for Advancing Translational Sciences, Natonal Institutes of Health.

References

1. Mahalingan, K.K., Keith Keenan, E., Strickland, M., Li, Y., Liu, Y., Ball, H.L., Tanner, M.E., Tjandra, N. and Roll-Mecak, A. (2020) Structural basis for polyglutamate chain initiation and elongation by TTLL family enzymes. *Nat. Struct. Mol. Biol.*, **27**, 802–813.
2. Janke, C. and Magiera, M.M. (2020) The tubulin code and its role in controlling microtubule properties and functions. *Nat. Rev. Mol. Cell. Biol.*, **21**, 307–326.
3. Janke, C., Rogowski, K. and van Dijk, J. (2008) Polyglutamylation: a fine-regulator of protein function? 'Protein modifications: beyond the usual suspects' review series. *EMBO Rep.*, **9**, 636–641.
4. Kann, M.L., Soues, S., Levilliers, N. and Fouquet, J.P. (2003) Glutamylated tubulin: diversity of expression and distribution of isoforms. *Cell Motil. Cytoskeleton*, **55**, 14–25.
5. van Dijk, J., Rogowski, K., Miro, J., Lacroix, B., Edde, B. and Janke, C. (2007) A targeted multienzyme mechanism for selective microtubule polyglutamylation. *Mol. Cell*, **26**, 437–448.
6. Zempel, H., Luedtke, J., Kumar, Y., Biernat, J., Dawson, H., Mandelkow, E. and Mandelkow, E.M. (2013) Amyloid-beta oligomers induce synaptic damage via tau-dependent microtubule severing by TTLL6 and spastin. *EMBO J.*, **32**, 2920–2937.
7. Janke, C., Rogowski, K., Wloga, D., Regnard, C., Kajava, A.V., Strub, J.M., Temurak, N., van Dijk, J., Boucher, D., van Dorsselaer, A. *et al.* (2005) Tubulin polyglutamylase enzymes are members of the TTL domain protein family. *Science*, **308**, 1758–1762.
8. Lacroix, B., van Dijk, J., Gold, N.D., Guizetti, J., Aldrian-Herrada, G., Rogowski, K., Gerlich, D.W. and Janke, C. (2010) Tubulin polyglutamylation stimulates spastin-mediated microtubule severing. *J. Cell Biol.*, **189**, 945–954.
9. Wloga, D., Dave, D., Meagley, J., Rogowski, K., Jerka-Dziadosz, M. and Gaertig, J. (2010) Hyperglutamylation of tubulin can either stabilize or destabilize microtubules in the same cell. *Eukaryot. Cell*, **9**, 184–193.
10. Suryavanshi, S., Edde, B., Fox, L.A., Guerrero, S., Hard, R., Hennessey, T., Kabi, A., Malison, D., Pennock, D., Sale, W.S. *et al.* (2010) Tubulin glutamylation regulates ciliary motility by altering inner dynein arm activity. *Curr. Biol.*, **20**, 435–440.
11. Pathak, N., Obara, T., Mangos, S., Liu, Y. and Drummond, I.A. (2007) The zebrafish fleer gene encodes an essential regulator of cilia tubulin polyglutamylation. *Mol. Biol. Cell*, **18**, 4353–4364.
12. Pathak, N., Austin, C.A. and Drummond, I.A. (2011) Tubulin tyrosine ligase-like genes ttll3 and ttll6 maintain zebrafish cilia structure and motility. *J. Biol. Chem.*, **286**, 11685–11695.
13. Bosch Grau, M., Gonzalez Curto, G., Rocha, C., Magiera, M.M., Marques Sousa, P., Giordano, T., Spassky, N. and Janke, C. (2013) Tubulin glycylases and glutamylases have distinct functions in stabilization and motility of ependymal cilia. *J. Cell Biol.*, **202**, 441–451.
14. Lee, J.E., Silhavy, J.L., Zaki, M.S., Schroth, J., Bielas, S.L., Marsh, S.E., Olvera, J., Brancati, F., Iannicelli, M., Ikegami, K. *et al.* (2012) CEP41 is mutated in Joubert syndrome and is required for tubulin glutamylation at the cilium. *Nat. Genet.*, **44**, 193–199.
15. He, K., Ma, X., Xu, T., Li, Y., Hodge, A., Zhang, Q., Torline, J., Huang, Y., Zhao, J., Ling, K. *et al.* (2018) Axoneme polyglutamylation regulated by Joubert syndrome protein ARL13B controls ciliary targeting of signaling molecules. *Nat. Commun.*, **9**, 3310.
16. Zempel, H. and Mandelkow, E.M. (2015) Tau missorting and spastin-induced microtubule disruption in neurodegeneration: Alzheimer disease and hereditary spastic paraplegia. *Mol. Neurodegener.*, **10**, 68.
17. Jean, D.C. and Baas, P.W. (2013) It cuts two ways: microtubule loss during Alzheimer disease. *EMBO J.*, **32**, 2900–2902.
18. Xia, P., Ye, B., Wang, S., Zhu, X., Du, Y., Xiong, Z., Tian, Y. and Fan, Z. (2016) Glutamylation of the DNA sensor cGAS regulates its binding and synthase activity in antiviral immunity. *Nat. Immunol.*, **17**, 369–378.
19. Ye, B., Li, C., Yang, Z., Wang, Y., Hao, J., Wang, L., Li, Y., Du, Y., Hao, L., Liu, B. *et al.* (2014) Cytosolic carboxypeptidase CCP6 is required for megakaryopoiesis by modulating Mad2 polyglutamylation. *J. Exp. Med.*, **211**, 2439–2454.
20. Lee, K., Tirasophon, W., Shen, X., Michalak, M., Prywes, R., Okada, T., Yoshida, H., Mori, K. and Kaufman, R.J. (2002) IRE1-mediated unconventional mRNA splicing and S2P-mediated ATF6 cleavage merge to regulate XBP1 in signaling the unfolded protein response. *Genes Dev.*, **16**, 452–466.
21. Yoshida, H., Matsui, T., Yamamoto, A., Okada, T. and Mori, K. (2001) XBP1 mRNA is induced by ATF6 and spliced by IRE1 in response to ER stress to produce a highly active transcription factor. *Cell*, **107**, 881–891.
22. Zhong, Y., Yan, W., Ruan, J., Fang, M., Lapidus, R.G., Du, S. and Fang, S. (2021) A novel XBP1 variant is highly enriched in cancer tissues and is specifically required for cancer cell survival. *Biochem. Biophys. Res. Commun.*, **562**, 69–75.
23. Cross, B.C., Bond, P.J., Sadowski, P.G., Jha, B.K., Zak, J., Goodman, J.M., Silverman, R.H., Neubert, T.A., Baxendale, I.R., Ron, D. *et al.* (2012) The molecular basis for selective inhibition of unconventional mRNA splicing by an IRE1-binding small molecule. *Proc. Natl. Acad. Sci. U. S. A.*, **109**, E869–E878.
24. Calfon, M., Zeng, H., Urano, F., Till, J.H., Hubbard, S.R., Harding, H.P., Clark, S.G. and Ron, D. (2002) IRE1 couples endoplasmic reticulum load to secretory capacity by processing the XBP-1 mRNA. *Nature*, **415**, 92–96.
25. Tsuchiya, Y., Saito, M., Kadokura, H., Miyazaki, J.I., Tashiro, F., Imagawa, Y., Iwawaki, T. and Kohno, K. (2018) IRE1-XBP1 pathway

regulates oxidative proinsulin folding in pancreatic beta cells. *J. Cell Biol.*, **217**, 1287–1301.
26. Tsuru, A., Fujimoto, N., Takahashi, S., Saito, M., Nakamura, D., Iwano, M., Iwawaki, T., Kadokura, H., Ron, D. and Kohno, K. (2013) Negative feedback by IRE1beta optimizes mucin production in goblet cells. *Proc. Natl. Acad. Sci. U. S. A.*, **110**, 2864–2869.
27. Deng, M., Bragelmann, J., Kryukov, I., Saraiva-Agostinho, N. and Perner, S. (2017) FirebrowseR: an R client to the broad Institute's firehose pipeline. *Database*, **2017**, baw160.
28. Bertolotti, A. and Ron, D. (2001) Alterations in an IRE1-RNA complex in the mammalian unfolded protein response. *J. Cell Sci.*, **114**, 3207–3212.
29. Feldman, H.C., Vidadala, V.N., Potter, Z.E., Papa, F.R., Backes, B.J. and Maly, D.J. (2019) Development of a chemical toolset for studying the paralog-specific function of IRE1. *ACS Chem. Biol.*, **14**, 2595–2605.
30. Yoshida, H., Oku, M., Suzuki, M. and Mori, K. (2006) pXBP1(U) encoded in XBP1 pre-mRNA negatively regulates unfolded protein response activator pXBP1(S) in mammalian ER stress response. *J. Cell Biol.*, **172**, 565–575.
31. Hanzelmann, S., Castelo, R. and Guinney, J. (2013) GSVA: gene set variation analysis for microarray and RNA-seq data. *BMC Bioinformatics*, **14**, 7.
32. Subramanian, A., Tamayo, P., Mootha, V.K., Mukherjee, S., Ebert, B.L., Gillette, M.A., Paulovich, A., Pomeroy, S.L., Golub, T.R., Lander, E.S. *et al.* (2005) Gene set enrichment analysis: a knowledge-based approach for interpreting genome-wide expression profiles. *Proc. Natl. Acad. Sci. U. S. A.*, **102**, 15545–15550.
33. Lee, A.H., Iwakoshi, N.N. and Glimcher, L.H. (2003) XBP-1 regulates a subset of endoplasmic reticulum resident chaperone genes in the unfolded protein response. *Mol. Cell. Biol.*, **23**, 7448–7459.
34. Hellman, L.M. and Fried, M.G. (2007) Electrophoretic mobility shift assay (EMSA) for detecting protein-nucleic acid interactions. *Nat. Protoc.*, **2**, 1849–1861.
35. Bobinnec, Y., Moudjou, M., Fouquet, J.P., Desbruyeres, E., Edde, B. and Bornens, M. (1998) Glutamylation of centriole and cytoplasmic tubulin in proliferating non-neuronal cells. *Cell Motil. Cytoskeleton*, **39**, 223–232.
36. Vemu, A., Szczesna, E., Zehr, E.A., Spector, J.O., Grigorieff, N., Deaconescu, A.M. and Roll-Mecak, A. (2018) Severing enzymes amplify microtubule arrays through lattice GTP-tubulin incorporation. *Science*, **361**, eaau1504.
37. Kuo, Y.W., Trottier, O., Mahamdeh, M. and Howard, J. (2019) Spastin is a dual-function enzyme that severs microtubules and promotes their regrowth to increase the number and mass of microtubules. *Proc. Natl. Acad. Sci. U. S. A.*, **116**, 5533–5541.
38. Zanic, M., Stear, J.H., Hyman, A.A. and Howard, J. (2009) EB1 recognizes the nucleotide state of tubulin in the microtubule lattice. *PLoS One*, **4**, e7585.
39. Maurer, S.P., Fourniol, F.J., Bohner, G., Moores, C.A. and Surrey, T. (2012) EBs recognize a nucleotide-dependent structural cap at growing microtubule ends. *Cell*, **149**, 371–382.
40. Maurer, S.P., Bieling, P., Cope, J., Hoenger, A. and Surrey, T. (2011) GTPgammaS microtubules mimic the growing microtubule end structure recognized by end-binding proteins (EBs). *Proc. Natl. Acad. Sci. U. S. A.*, **108**, 3988–3993.
41. Janke, C. and Montagnac, G. (2017) Causes and consequences of microtubule acetylation. *Curr. Biol.*, **27**, R1287–R1292.
42. Salmon, E.D. and Begg, D.A. (1980) Functional implications of cold-stable microtubules in kinetochore fibers of insect spermatocytes during anaphase. *J. Cell Biol.*, **85**, 853–865.
43. Dominguez-Brauer, C., Thu, K.L., Mason, J.M., Blaser, H., Bray, M.R. and Mak, T.W. (2015) Targeting mitosis in Cancer: emerging strategies. *Mol. Cell*, **60**, 524–536.
44. Otto, T. and Sicinski, P. (2017) Cell cycle proteins as promising targets in cancer therapy. *Nat. Rev. Cancer*, **17**, 93–115.
45. Kahles, A., Lehmann, K.V., Toussaint, N.C., Huser, M., Stark, S.G., Sachsenberg, T., Stegle, O., Kohlbacher, O., Sander, C., Cancer Genome Atlas Research, N. *et al.* (2018) Comprehensive analysis of alternative splicing across Tumors from 8,705 patients. *Cancer Cell*, **34**, 211, e216–224.
46. Demircioglu, D., Cukuroglu, E., Kindermans, M., Nandi, T., Calabrese, C., Fonseca, N.A., Kahles, A., Lehmann, K.V., Stegle, O., Brazma, A. *et al.* (2019) A pan-cancer transcriptome analysis reveals pervasive regulation through alternative promoters. *Cell*, **178**, 1465, e1417–1477.
47. Bertolotti, A., Zhang, Y., Hendershot, L.M., Harding, H.P. and Ron, D. (2000) Dynamic interaction of BiP and ER stress transducers in the unfolded-protein response. *Nat. Cell Biol.*, **2**, 326–332.
48. Martino, M.B., Jones, L., Brighton, B., Ehre, C., Abdulah, L., Davis, C.W., Ron, D., O'Neal, W.K. and Ribeiro, C.M. (2013) The ER stress transducer IRE1beta is required for airway epithelial mucin production. *Mucosal Immunol.*, **6**, 639–654.
49. Iqbal, J., Dai, K., Seimon, T., Jungreis, R., Oyadomari, M., Kuriakose, G., Ron, D., Tabas, I. and Hussain, M.M. (2008) IRE1beta inhibits chylomicron production by selectively degrading MTP mRNA. *Cell Metab.*, **7**, 445–455.
50. Imagawa, Y., Hosoda, A., Sasaka, S., Tsuru, A. and Kohno, K. (2008) RNase domains determine the functional difference between IRE1alpha and IRE1beta. *FEBS Lett.*, **582**, 656–660.
51. Grey, M.J., Cloots, E., Simpson, M.S., LeDuc, N., Serebrenik, Y.V., De Luca, H., De Sutter, D., Luong, P., Thiagarajah, J.R., Paton, A.W. *et al.* (2020) IRE1beta negatively regulates IRE1alpha signaling in response to endoplasmic reticulum stress. *J. Cell Biol.*, **219**, e201904048.
52. Iwawaki, T., Hosoda, A., Okuda, T., Kamigori, Y., Nomura-Furuwatari, C., Kimata, Y., Tsuru, A. and Kohno, K. (2001) Translational control by the ER transmembrane kinase/ribonuclease IRE1 under ER stress. *Nat. Cell Biol.*, **3**, 158–164.
53. Yanagitani, K., Imagawa, Y., Iwawaki, T., Hosoda, A., Saito, M., Kimata, Y. and Kohno, K. (2009) Cotranslational targeting of XBP1 protein to the membrane promotes cytoplasmic splicing of its own mRNA. *Mol. Cell*, **34**, 191–200.
54. Yanagitani, K., Kimata, Y., Kadokura, H. and Kohno, K. (2011) Translational pausing ensures membrane targeting and cytoplasmic splicing of XBP1u mRNA. *Science*, **331**, 586–589.
55. Shanmuganathan, V., Schiller, N., Magoulopoulou, A., Cheng, J., Braunger, K., Cymer, F., Berninghausen, O., Beatrix, B., Kohno, K., von Heijne, G. *et al.* (2019) Structural and mutational analysis of the ribosome-arresting human XBP1u. *elife*, **8**, e46267.
56. Sundaram, A., Plumb, R., Appathurai, S. and Mariappan, M. (2017) The Sec61 translocon limits IRE1alpha signaling during the unfolded protein response. *elife*, **6**, e27187.
57. Abal, M., Keryer, G. and Bornens, M. (2005) Centrioles resist forces applied on centrosomes during G2/M transition. *Biol. Cell.*, **97**, 425–434.
58. McNally, F.J., Okawa, K., Iwamatsu, A. and Vale, R.D. (1996) Katanin, the microtubule-severing ATPase, is concentrated at centrosomes. *J. Cell Sci.*, **109**(Pt 3), 561–567.
59. Hartman, J.J., Mahr, J., McNally, K., Okawa, K., Iwamatsu, A., Thomas, S., Cheesman, S., Heuser, J., Vale, R.D. and McNally, F.J. (1998) Katanin, a microtubule-severing protein, is a novel AAA

ATPase that targets to the centrosome using a WD40-containing subunit. *Cell*, **93**, 277–287.
60. McNally, F.J. and Roll-Mecak, A. (2018) Microtubule-severing enzymes: from cellular functions to molecular mechanism. *J. Cell Biol.*, **217**, 4057–4069.
61. Maruta, H., Greer, K. and Rosenbaum, J.L. (1986) The acetylation of alpha-tubulin and its relationship to the assembly and disassembly of microtubules. *J. Cell Biol.*, **103**, 571–579.
62. Bulinski, J.C., Richards, J.E. and Piperno, G. (1988) Posttranslational modifications of alpha tubulin: detyrosination and acetylation differentiate populations of interphase microtubules in cultured cells. *J. Cell Biol.*, **106**, 1213–1220.
63. Akella, J.S., Wloga, D., Kim, J., Starostina, N.G., Lyons-Abbott, S., Morrissette, N.S., Dougan, S.T., Kipreos, E.T. and Gaertig, J. (2010) MEC-17 is an alpha-tubulin acetyltransferase. *Nature*, **467**, 218–222.
64. Shida, T., Cueva, J.G., Xu, Z., Goodman, M.B. and Nachury, M.V. (2010) The major alpha-tubulin K40 acetyltransferase alphaTAT1 promotes rapid ciliogenesis and efficient mechanosensation. *Proc. Natl. Acad. Sci. U. S. A.*, **107**, 21517–21522.
65. Godek, K.M., Kabeche, L. and Compton, D.A. (2015) Regulation of kinetochore-microtubule attachments through homeostatic control during mitosis. *Nat. Rev. Mol. Cell. Biol.*, **16**, 57–64.
66. Vitale, I., Galluzzi, L., Castedo, M. and Kroemer, G. (2011) Mitotic catastrophe: a mechanism for avoiding genomic instability. *Nat. Rev. Mol. Cell. Biol.*, **12**, 385–392.
67. Zierhut, C., Yamaguchi, N., Paredes, M., Luo, J.D., Carroll, T. and Funabiki, H. (2019) The cytoplasmic DNA sensor cGAS promotes mitotic cell death. *Cell*, **178**, 302, e323–315.
68. Hong, S.Y. and Hagen, T. (2013) Multiple myeloma Leu167Ile (c.499C>a) mutation prevents XBP1 mRNA splicing. *Br. J. Haematol.*, **161**, 898–901.
69. Jiang, H., Lei, R., Ding, S.W. and Zhu, S. (2014) Skewer: a fast and accurate adapter trimmer for next-generation sequencing paired-end reads. *BMC Bioinformatics*, **15**, 182.
70. Kim, D., Langmead, B. and Salzberg, S.L. (2015) HISAT: a fast spliced aligner with low memory requirements. *Nat. Methods*, **12**, 357–360.
71. Liao, Y., Smyth, G.K. and Shi, W. (2014) featureCounts: an efficient general purpose program for assigning sequence reads to genomic features. *Bioinformatics*, **30**, 923–930.
72. Robinson, M.D., McCarthy, D.J. and Smyth, G.K. (2010) edgeR: a Bioconductor package for differential expression analysis of digital gene expression data. *Bioinformatics*, **26**, 139–140.
73. Ritchie, M.E., Phipson, B., Wu, D., Hu, Y., Law, C.W., Shi, W. and Smyth, G.K. (2015) Limma powers differential expression analyses for RNA-sequencing and microarray studies. *Nucleic Acids Res.*, **43**, e47.
74. Vivian, J., Rao, A.A., Nothaft, F.A., Ketchum, C., Armstrong, J., Novak, A., Pfeil, J., Narkizian, J., Deran, A.D., Musselman-Brown, A. *et al.* (2017) Toil enables reproducible, open source, big biomedical data analyses. *Nat. Biotechnol.*, **35**, 314–316.
75. Hall, M.P., Unch, J., Binkowski, B.F., Valley, M.P., Butler, B.L., Wood, M.G., Otto, P., Zimmerman, K., Vidugiris, G., Machleidt, T. *et al.* (2012) Engineered luciferase reporter from a deep sea shrimp utilizing a novel imidazopyrazinone substrate. *ACS Chem. Biol.*, **7**, 1848–1857.
76. De Conto, F., Di Lonardo, E., Arcangeletti, M.C., Chezzi, C., Medici, M.C. and Calderaro, A. (2012) Highly dynamic microtubules improve the effectiveness of early stages of human influenza a/NWS/33 virus infection in LLC-MK2 cells. *PLoS One*, **7**, e41207.
77. Bell, P.B., Jr. and Safiejko-Mroczka, B. (1995) Improved methods for preserving macromolecular structures and visualizing them by fluorescence and scanning electron microscopy. *Scanning Microsc.*, **9**, 843–857 discussion 858-860.
78. Lampson, M.A. and Kapoor, T.M. (2005) The human mitotic checkpoint protein BubR1 regulates chromosome-spindle attachments. *Nat. Cell Biol.*, **7**, 93–98.